ISSN: 1343-4292
Volume 142, Issue 09, September, 2024

In Silico Homology Modeling and Binding Analysis of ESAT-6 in *Mycobacterium tuberculosis*: Structural Insights and Interaction with MHC Class II HLA-DR Subunits

Nathan Rhoey Fababier[1], Charimaine Joy Cuervo[2], Juliana Jei Datuon[3], John Kieffer David[4], Alexa Bianca De Castro[5], Larina Dee Dela Peña[6], Marie Louvina Mae Domingo[7], Earl Adriane Cano[8]

Department of Medical Technology, Institute of Health Sciences and Nursing, Far Eastern University, Manila, Philippines[1,2,3,4,5,6,7,8]

ABSTRACT— Tuberculosis (TB) remains a global health concern, particularly in developing countries, with *Mycobacterium tuberculosis* (*M. tb*) as its main causative agent. The 6 kDa Early Secreted Antigenic Target (ESAT-6) protein serves a function in *M. tb* virulence by disrupting phagosomal membranes and evading immune detection. This study employs in silico techniques to analyze the physicochemical properties, structural characteristics, and binding interactions of ESAT-6 with major histocompatibility complex (MHC) class II HLA-DR subunits. Rendering the model was done using SWISS-MODEL integrated with model validity parameters (i.e. QMEAN, Ramachandran Plot Analysis and MolProbity) which exhibited results proving the rendered model was reliable though with a few discrepancies. ESAT-6 exhibited hydrophilic and hydrophobic sides and aliphatic molecules in its core that influenced its functional properties. Physicochemical properties and secondary structures were characterized using ProtParam, ProtScale, and NetSurfP 3.0. Moreover, it was found that the majority of the protein has >25% relative surface area (RSA) with its N-terminal and C-terminal regions being the most exposed. Using ClusPro and PRODIGY for molecular docking, HLA-DRB3 exhibited the highest affinity to ESAT-6 (ΔG = -11.4 kcal/mol; $K_d = 9.4\times10^{-9}$), suggesting a role in the host's immune response. The apolar-apolar interfacial contacts (ICs) contributed to most of the binding energy with evidence of consistent binding motifs between ESAT-6 and the HLA-DRB3.

KEYWORDS: ESAT-6, homology modeling, MHC Class II, binding affinity, tuberculosis

DOI:
09.10554/Bnihs.29.09.2024.01

1. Introduction

Tuberculosis (TB) is still a prevailing global health crisis, especially in developing countries. TB is an infectious airborne disease affecting the lungs that can be transmitted when a TB patient talks, sneezes, or coughs, causing tiny droplets to be suspended in the air and when inhaled, could lead to manifesting the disease [1]. In a report, the World Health Organization (WHO) indicated that an estimation of 10.8 million people suffered from TB in 2023 globally, inevitably present in various age brackets and every country [2]. Additionally, 1.25 million people succumbed to TB in the same year.

Its main causative agent, *Mycobacterium tuberculosis* (*M. tb*), is a persistent pathogen that lingers until an opening for infection arises. This pathogen utilizes the host's macrophages to survive rather than relying on

virulent factors such as capsules, toxins, pili, or flagella and to transport the pathogen into the lung parenchyma and other tissues by establishing intracellular niches on the cell [3]. The major virulence factor of *M. tb* comes from a protein it secretes called the 6 kDa Early Secreted Antigenic Target (ESAT-6) [4]. This protein is believed to be encoded by the Region of Difference 1 (RD1) of *M. tb*, which is crucial for its virulence and pathogenicity inside the host. When inside the phagosome, the ESAT-6 disrupts the phagosomal membrane, allowing the pathogen to escape. Since the protein translocates in the endoplasmic reticulum, it can prevent antigen presentation of major histocompatibility complex (MHC) class 1 to the macrophage by interacting with β-2-microglobulin [3].

Moreover, a system of genes that significantly contributes to antigen recognition through coding for cell-surface molecules is called MHC. MHC molecules' main function is for antigen presentation for T cell recognition and activation, a reason why it is found mainly on antigen presenting cells. Additionally, it is found to be the most polymorphic system allowing immune response to various immunogens for survival [5]. MHC has two classes: class I and class II. Class I are evident in A, B, and C various loci or locations while class II are found in the D region with further loci termed as DR, DQ, and DP.

Furthermore, cultured ELISPOT and ex vivo analysis was done, and HLA-DR shows notably high CD4+ T cell response to *M. tb* than HLA DQ and HLA-DP, where HLA-DR-restricted T cells are selected eminently against pathogens [6]. Hereby, this study intends to analyze the binding of ESAT-6 in *M. tb* through in silico homology modeling and assess its structural insights and interaction with MHC class II HLA-DR subunits.

2. Methodology

2.1 Protein Retrieval

The protein sequence of ESAT-6 and HLA-DR subunits were acquired from UniProt and ensured to be of human origin and reviewed by UniProtKB [7]. The HLA-DR subunits used in this study are the following with their respective UniProt accession number: HLA-DRA (P01903), HLA-DRB1 (P01911), HLA-DRB3 (P79483), HLA-DRB4 (P13762), and HLA-DRB5 (Q30154). These proteins were used to bind with ESAT-6 (P9WNK7) in anticipation of understanding its role in hindering the virulence of the pathogen.

2.2 Homology Modeling and Model Validation

To meet the objectives of the study, a homology modeling of the protein ESAT-6 was constructed using SWISS-MODEL [8], [9]. The researchers identified the physical characteristics of the protein by rendering its 3D structure that aided in the virulence factor of the pathogen *M. tb*.

After homology modeling, ESAT-6 was subjected for model validation using the model quality metrics in SWISS-MODEL. The Ramachandran Plot Analysis in SWISS-MODEL was used to assess the quality of the predicted model of ESAT-6 protein [10]. Additionally, the structural assessment of ESAT-6 could also be conducted based on the MolProbity results generated by SWISS-MODEL [11]. MolProbity score, Clash Score, Rotamer Outliers, C-beta Deviations, Bad Bonds, and Bad Angles were obtained and evaluated. Furthermore, the QMEAN and QMEANDisCo were also obtained to assess the quality of the model.

Moreover, to validate the modeling of the ESAT-6 protein, NetSurfP 3.0 was utilized to predict its structural features based on its amino acid sequence [12]. The dihedral angles of ESAT-6's backbone are represented as the "phi angles" and "psi angles" and were used for the validation of secondary structures. Additionally, regions lacking defined structure were identified as areas of structural disorders.

ISSN: 1343-4292
Volume 142, Issue 09, September, 2024

2.3 Sequence-based and Structural Analysis

This study utilized ProtParam as a tool for the calculation of different physical and chemical properties of ESAT-6 [13]. The program computed the total number of amino acids, atoms, and number of negatively charged residues. It also determined its molecular weight and atomic composition, theoretical PI, extinction coefficients, estimated half-life, aliphatic and instability index, and grand average of hydropathicity or (GRAVY) [11]. Additionally, the hydropathy plots of ESAT-6, based on Kyte and Doolittle hydropathy scale, were determined by Expasy's Protscale tool [13].

Furthermore, NetSurfP 3.0 predicted secondary structures and solvent accessibility, and identified regions with distinct structures. The tool also provided a spreadsheet of the protein's individual residues with their corresponding relative surface area (RSA) and their absolute surface area, which was used to interpret the potential binding sites for host proteins [12]. The disordered regions were listed here as well. Data regarding each residue's prediction on what secondary structures it would most likely form were also included, while also providing more specific subsets of structures like 310 helices and α-helices under helical structures.

2.4 Molecular Docking and Functional Analysis

HLA-DR subunits were utilized to examine its interaction with ESAT-6. The residues of HLA-DR subunits involved in the transmembrane helices were identified using the server DeepTMHMM - 1.0 [14] and were manually removed and constructed using the homology modeling method, specifically utilizing the SWISS-MODEL, to obtain its pdb file. ClusPro was used for the docking of HLA-DR subunit and ESAT-6 [15-19]. The top-ranking model simulated under the Balanced Scoring Coefficients had its pdb file downloaded and inputted to PRODIGY, which released the results for the binding affinity, dissociation constants, interfacial contacts, and residue pairs contributing to the binding of the protein-protein molecules [20- 22]. The researchers set the temperature to 37°C to mimic the body's core physiological temperature for an optimal metabolic process [23]. Furthermore, ChimeraX was used to visualize the protein-protein complex [24- 26]. The residue pairs identified by PRODIGY were used to determine binding motifs, which were visualized by aligning the protein sequences of ESAT-6 and the five HLA-DR subunits.

3. Results and Discussion

3.1 Sequence-based and Structural Analysis

3.1.1 Physicochemical Properties of ESAT-6

The data provided by ProtParam described ESAT-6 as a protein with a total of 95 amino acids, a molecular weight of approximately 9904 Da, and a theoretical isoelectric point of 4.48. The amino acid composition revealed a predominance of alanine (17.9%), glycine (10.5%), and glutamine (9.5%). The high proportion of alanine and glycine contributed to the flexibility and potential structural motifs within the protein. For instance, glycine's small side chain allows for tighter turns in polypeptides, which maintains the structural integrity in compact folds or loops [27]. In contrast, the presence of nine negatively charged residues and four positively charged residues inferred that this protein has a relatively neutral charge at physiological pH, which influenced its interaction with host immune components. A neutral charge reduced strong repulsive or attractive electrostatic interactions with surrounding biomolecules. This enabled ESAT-6 to engage more subtly with host cells and immune components without triggering an overt immune response [28].

The instability index calculated at 36.36 classified this protein as stable which was critical for proteins involved in immune evasion who seeked to persist in host environments to exert their effects. Moreover, the estimated half-life of 30 hours in mammalian reticulocytes indicates that this protein remains functional for

extended periods, allowing it to play a role in chronic infections [29].

Additionally, the aliphatic index of 72.21 indicated a significant proportion of aliphatic amino acids, which typically contributed to the stability and structural integrity of proteins. The stability of ESAT-6 was essential to maintain its structure while interacting with host cells, even under varying conditions such as pH or temperature [28]. On the other hand, the extinction coefficient at 280 nm of 17990 M^{-1} cm^{-1} indicated that this protein has a high absorbance at this wavelength, likely due to the presence of aromatic residues such as phenylalanine and tyrosine. The presence of three tryptophan residues, one tyrosine residue, and two phenylalanine residues in ESAT-6 sufficiently accounted for the observed extinction coefficient at 280 nm. This property could be utilized for quantifying protein concentration in various assays [29]. The flexibility imparted by high levels of alanine and glycine allowed ESAT-6 to adopt multiple conformations that enhance its ability to bind to host receptors or evade detection by immune surveillance mechanisms [30]. Alanine and glycine residues conferred localized flexibility in regions such as loops, turns, or surface-exposed areas, facilitating dynamic interactions and conformational adaptability. In contrast, aliphatic residues such as valine, leucine, and isoleucine contributed to the formation of a stable hydrophobic core, which supports the maintenance of the protein's overall structure and functionality. This dual characteristic ensured the protein adapted to varying environmental conditions while preserving its structural integrity [31].

Furthermore, the GRAVY value of -0.256 suggested that the protein is relatively hydrophilic. This property is often associated with proteins that interacted with aqueous environments or cellular surfaces, which was consistent with ESAT-6's role in modulating immune responses [32].

The ability of ESAT-6 to maintain a stable yet flexible conformation enabled its persistence within the host environment while facilitating evasion of immune surveillance. These findings offered valuable insights into the molecular mechanisms underlying ESAT-6 activity, which could inform the development of therapeutic strategies aimed at disrupting its structural integrity or interactions with host factors to mitigate TB infection.

3.1.2 Hydropathy Scale

Table 1 Hydropathicity by Kyte and Doolittle with Percentages of ESAT-6 Composition

Nonpolar	Score	ESAT-6 (%)	Polar	Score	ESAT-6 (%)	Charged	Score	ESAT-6 (%)
Ala	1.8	17 (17.9%)	Asn	-3.5	6 (6.3%)	Arg	-4.5	1 (1.1%)
Gly	-0.4	10 (10.5%)	Cys	2.5	0 (0.0%)	Asp	-3.5	2 (2.1%)
Ile	4.5	4 (4.2%)	Gln	-3.5	9 (9.5%)	Glu	-3.5	7 (7.4%)
Leu	3.8	7 (7.4%)	Met	1.9	3 (3.2%)	His	-3.2	1 (1.1%)
Phe	2.8	2 (2.1%)	Ser	-0.8	8 (8.4%)	Lys	-3.9	3 (3.2%)
Pro	-1.6	0 (0.0%)	Thr	-0.7	8 (8.4%)			
Trp	-0.9	3 (3.2%)						
Tyr	-1.3	1 (1.1%)						

ISSN: 1343-4292
Volume 142, Issue 09, September, 2024

Val	4.2	3 (3.2%)		

The Kyte-Doolittle hydropathy scale is essential for identifying specific regions within proteins that exhibit significant motifs based on their hydrophobicity and hydrophilicity. Regions with positive hydropathy values indicated hydrophobic segments, which are often associated with transmembrane domains or internal areas of globular proteins. For instance, amino acids like isoleucine (4.5), valine (4.2), and leucine (3.8) are highly hydrophobic, suggesting that stretches of these residues formed transmembrane helices if they appear consecutively in a protein sequence. This concept had been previously established, reinforcing the notion that ESAT-6 possesses transmembrane capabilities. The ESAT-6 interacted with membranes, exhibiting membrane-lytic activity and forming pores essential for its virulence [33]. Conversely, regions with negative values such as arginine (-4.5) and aspartic acid (-3.5) indicated hydrophilic residues likely to be surface-exposed and interacting with the aqueous environment. Most of the amino acid compositions in ESAT-6 consisted of alanine, glycine, and glutamine. Alanine was the most abundant with a hydropathy score of 1.8, indicating its hydrophobic nature. Glycine, the second most prominent, had a -0.4 hydropathy score which explained its relative neutrality in hydrophobicity. Then, glutamine had a -3.5 hydropathy score which identified it as hydrophilic. This distribution suggested that ESAT-6 has a mix of hydrophobic and hydrophilic regions, which influenced its structural and functional properties.

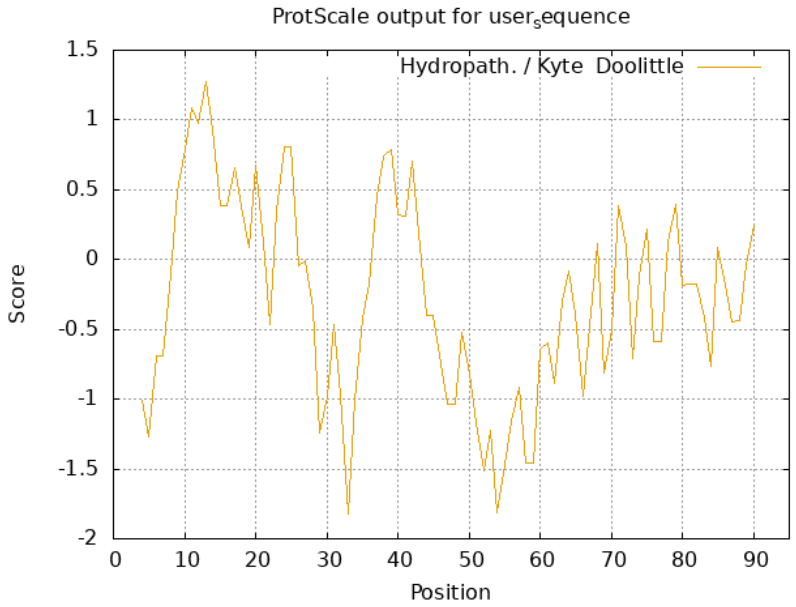

Figure 1 ProtScale Hydropathy Output Model

The analysis of hydropathy scores using the ProtScale revealed important insights into protein structure and function. For instance, consistently positive values at positions such as Gly-10 (0.789), Gly-20 (0.678), Ala-40 (0.322), and Val-90 (0.244) suggested the presence of a hydrophobic α-helix that likely spans a lipid bilayer. This implied that these regions are well-suited for interaction with the hydrophobic core of membranes. In contrast, segments with high negative values such as those at positions 30 (-0.978), 50 (-0.822), 60 (-0.644), 70 (-0.500), and 80 (-0.189), indicated loops or turns that were more likely to be in contact with the solvent. These hydrophilic regions are crucial for protein functionality, facilitating interactions with the aqueous environment and contributing to the overall dynamics of the protein structure [34].

3.1.3 Functional Regions

3.1.3.1 Secondary Structures

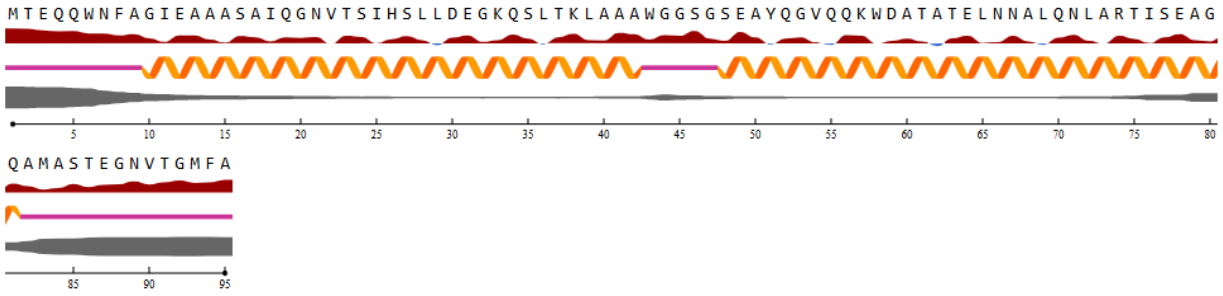

Figure 2 Graphical Representation of ESAT-6 using NetSurfP 3.0

Figure 2 represents ESAT-6's various amino acid conformation, with a "helix" seen as the orange coiled lines and a "coil" represented as a purple straight line. Upon observation, coiled strands were seen at the N-terminal and C-terminal ends. ESAT-6 started at a coiled strand with nine residues starting from Met-1 and ending in Ala-9. Changes in the conformation happen as it turns into a helix with 43 residues beginning at Gly-10 continuing until another alanine, the Ala-42. Furthermore, five more coiled residues make up the ESAT-6 sequence having Trp-43 at the beginning and Gly-47 as the end residue. These coiled residues were then replaced with helices starting from Ser-48, ending with Gln-81 residue constituting to 34 more residues but then altered again into coils at the last 14 residues having Ala-82 and Ala-95 as start and end amino acid residues, respectively. Helix strands constituted most of the ESAT-6 sequence since it has 65 helices out of 95 total residues or 68.42% of its whole conformation. In most of the helices, alanine, glycine, serine, and leucine were observed as these amino acids have greater tendencies of creating α-helices due to their capacity of generating hydrogen bonds derived from the polypeptide backbone [35]. When using an α-helix chain, glycine causes the bending of the sequence, which explains its presence in the start of most of the helix's regions of ESAT-6 [35]. The conformation of this protein generally depends on the interaction of its residues to each other and its depiction did not solely depend on the amino acid present in the certain residue number.

3.1.3.2 Relative Surface Accessibility (RSA) and Exposed Residues

The solvent accessibility of each residue in a protein sequence was analyzed to determine whether it is buried within the protein's interior or exposed to the surrounding environment. In NetSurfP 3.0, this was assessed as RSA, which is useful for identifying potential binding sites. Exposed residues are more likely to interact with other proteins or undergo conformational changes [36]. With a threshold of 25%, residues with an RSA below 25% were classified as "buried", while those with an RSA value above the threshold were considered "exposed" [12].

For ESAT-6, nine out of ninety-five residues fall below the 25% threshold, indicating that they are buried within the protein's structure, while the remaining eighty-six exposed residues were above 25% based on Figure 2. Additionally, the average RSA of the last ten residues at both N- and C- terminal ends was notably higher as compared to their adjacent sections. The average RSA for the N-terminal end spanning from Met-1 to Gly-10 was 74.50%, while the C-terminal end from Thr-86 to Ala-95 had an average RSA of 67.95%. These elevated values suggest that the terminal regions were the most exposed part of the protein.

Since exposed residues were more likely to interact with other molecules and undergo conformational changes [36]. The terminal ends of ESAT-6 highly contributed to its molecular recognition and binding

ISSN: 1343-4292
Volume 142, Issue 09, September, 2024

capacities. Their high RSA increases the likelihood of interactions with other proteins or molecules, potentially facilitating the formation of protein complexes or membrane anchoring. This implies that the terminal regions of ESAT-6 influenced the protein's functional properties and stability.

3.1.3.3 Disordered Regions

As shown in Figure 2, the disorder percentage was depicted as a gray line, with the line's thickness corresponding to the probability of a residue being disordered. The predicted model of ESAT-6 showed a thick line segment for the disorder percentage that gradually became thin until Ala-42, indicating a decreasing likelihood of disorder in the region. Trp-43 to Ser-48 residues exhibited a slightly higher disorder percentage as reflected by a thicker line segment. From this, the line segment became thin, representing lower disorder, and then gradually thickened again until Ala-95. This pattern suggested that the model had a higher percentage of disorder regions at its ends. Furthermore, this aligned with the local quality estimate of ESAT-6 (Figure 4) using SWISS-MODEL, which also indicated that the terminal ends have lower structural reliability compared to the core region [37].

Numerically, the disorder percentage for residues 1-7 and 83-95 exceeded the 50% median which indicates that these residues had the highest probability of being disordered. Conversely, the 57 to 66 residue exhibited <1%, suggesting they had the lowest probability of disorder. This made them the most stable regions and contained a fixed three-dimensional structure. Moreover, the flexible arms at the N- and C-terminal regions established transient dynamic interactions with lipid membranes that enabled the molecules to anchor into the membrane surface [37]. The disordered regions had the potential to interact with other proteins, aiding in the formation of protein complexes despite their lack of a stable structure. Thus, these regions are significant in binding and facilitating interactions with other molecules.

3.2 Homology Modeling and Model Validation

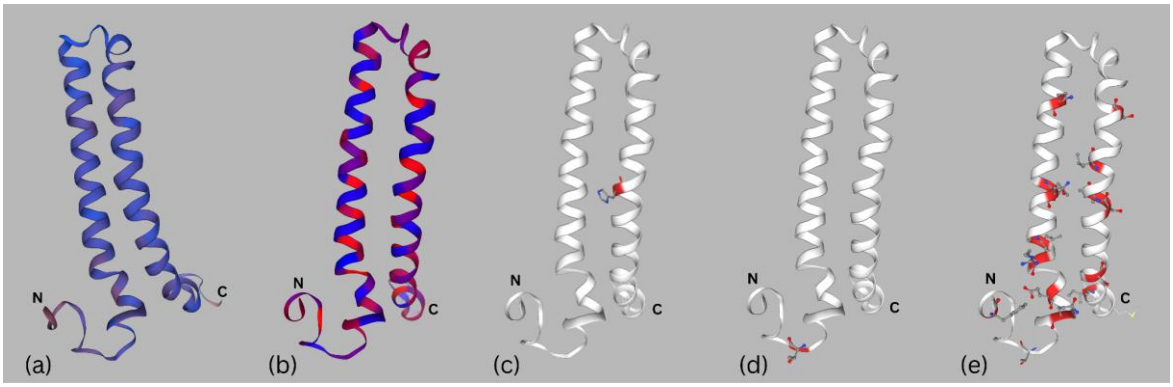

Figure 3 ESAT-6 Models using SWISS-MODEL. (a) Homology Model of ESAT-6 in SWISS-MODEL with Confidence Gradient (b) Model of ESAT-6 with Hydrophobicity Scale (c) Model of ESAT-6 with Bad Angles (d) Model of ESAT-6 with Rotamer Outliers (e) Model of ESAT-6 with Ramachandran Outliers

The resulting model of ESAT-6 revealed a structural arrangement comprising a combination of coils and helices (Figure 3a). The model displayed a confidence gradient, where red tones indicated regions of lower confidence, and blue tones signified regions of higher confidence. In the ESAT-6 model, residues located in the middle exhibit higher confidence, which gradually transitioned to lower confidence toward both ends.

Also, the model visualized the hydrophobicity of the residues, with regions of varying hydrophobicity represented by a color gradient (Figure 3b). Warm tones indicate regions with high hydrophobicity, while cool tones indicate regions that were least hydrophobic. Varying levels of hydrophobicity were observed,

with both terminal ends as hydrophobic regions. ESAT-6 exhibits a distinct hydrophobic and hydrophilic side, contributing to its various functions like forming associations with other proteins, including complexes or dimers/monomers [38]. The analysis of the hydrophobic side of the model revealed fourteen aliphatic amino acids with high hydrophobicity including four isoleucine, two alanine, seven leucine, and one valine. In contrast, the hydrophilic side of the model contained eighteen amino acids that are either uncharged amide or charged basic/acidic. These included six glutamine and two asparagine; one histidine, two lysine, and one arginine; two aspartate and three glutamate.

Bad angles in the model (Figure 3c) were also evaluated, specifically at residue B26-HIS, indicating a potential distortion in the backbone conformation that affected the overall structural integrity of the protein. Such deviations from ideal geometry compromised the functional interactions of ESAT-6 with host proteins, which is crucial for its role as a virulence factor [39].

Moreover, a notable rotamer outlier percentage of 22.06% was observed, affecting several residues including B55-GLN, B65-LEU, B74-ARG, B29-LEU, B72-LEU, B16-SER, B25-ILE, B78-GLU, B81-GLN, B66-ASN, B94-PHE, B24-SER, B35-SER, B11-ILE, B1-MET (Figure 3d). These outliers suggested a significant portion of the side chains not in their most favorable conformations, which were also located within helical regions. Helices underwent conformational adjustments, becoming more structured as α-helices under acidic conditions [37]. This misalignment hindered the protein's ability to interact effectively with its targets within the host immune system, potentially diminishing its pathogenicity.

Moreover, the Ramachandran plot analysis revealed that 1.08% of residues were classified as outliers, specifically at residue B86-THR (Figure 3e). While this percentage is relatively low, it still indicated some regions of conformational strain. The Ramachandran plot is a critical tool for assessing the stereochemical quality of protein models; thus, even minor deviations are indicative of underlying structural issues that warranted further investigation.

A MolProbity score of 2.14 suggests good structural quality, as it is close to the threshold for high-quality experimental models. This implies that the structure had relatively few errors in stereochemistry and geometry [40].

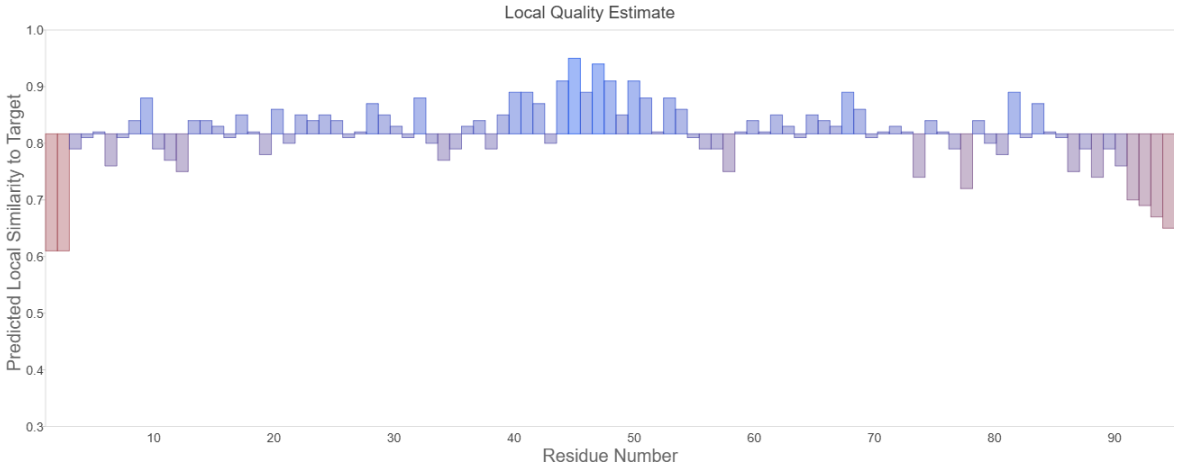

Figure 4 Local Quality Estimate of ESAT-6

Further, the QMEANDisCo Global score of 0.82 indicated a reliable representation of the true structure of the protein, as resulting scores closer to 1 reflected higher accuracy [8]. The local quality estimates

ISSN: 1343-4292
Volume 142, Issue 09, September, 2024

showcased a more detailed evaluation, predicting the similarity of each residue to the target structure. The fifty-four residues primarily located in the middle of the sequence achieved scores between 0.8-1.0, concluding a high local quality estimate that was reliable for downstream analyses (Figure 4) [8]. However, the remaining forty-one residues scored between 0.6-0.8 which suggested moderate reliability [8]. While these residues provided useful insights, they also expressed areas of the model with some degree of uncertainty. Sixteen of the forty-one residues were located at the terminal end which made these regions less structurally reliable compared to the core.

3.3 Molecular Docking

3.3.1 Binding Capacity of ESAT-6 to MHC class II HLA-DR subunits

Table 2 HLA-DR Subunits and ESAT-6 Docking Results via ClusPro

Protein-Protein Complex	Cluster	Members	Weighted Scores	
			Center	Lowest Energy
HLA-DRA:ESAT-6	0	113	-749.8	-876.4
HLA-DRB1:ESAT-6	0	147	-879.8	-1013.5
HLA-DRB3:ESAT-6	0	166	-832.5	-1023.6
HLA-DRB4:ESAT-6	0	114	-902.6	-1109.4
HLA-DRB5:ESAT-6	0	120	-854.9	-1002.5

Table 2 showed the members and weighted scores of each chosen HLA-DR subunit in complex with ESAT-6. The number of members, the weighted energy score of the center, and the lowest energy pertained to the size, the number of neighbor structures in the cluster, and the structure's energy score in the cluster, respectively [18], [22]. The best model cluster was chosen based on their lowest energy and binding affinity predicted using ClusPro.

Furthermore, Figure 5 showed the visualization of the docked protein-protein complex using ChimeraX. The HLA-DR subunits served as the receptor since it was the main target of the binding action between the proteins. These subunits were part of the MHC class II that bound antigenic peptides and presented them to CD4+ T cells [41]. HLA-DRA and HLA-DRB subunits formed the peptide-binding groove, which specifically bound foreign antigens [42]. On the other hand, the ESAT-6 served as the ligand that basically acted on the binding action with HLA-DR in a host. It activated the receptors that then stimulated the maturation of antigen presenting cells [30].

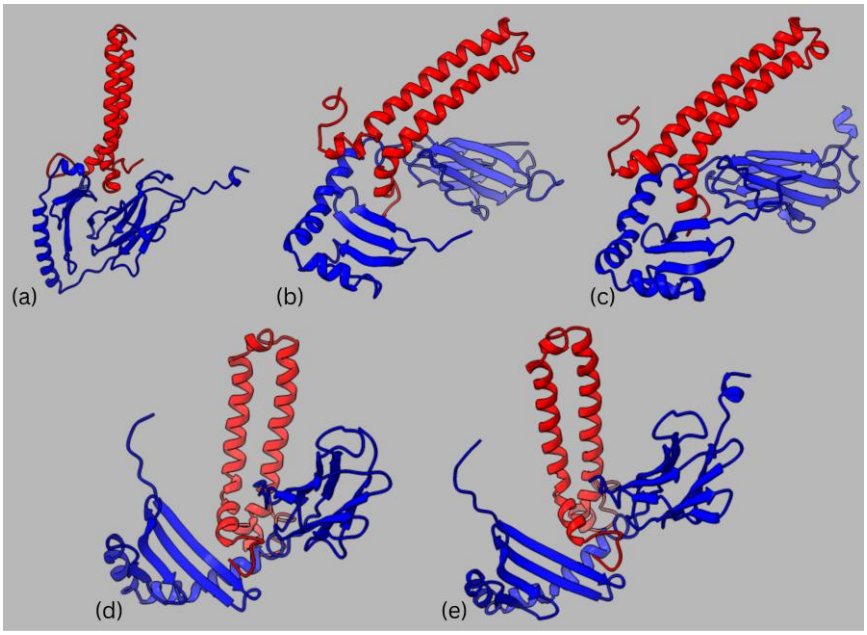

Figure 5 3D Models of ESAT-6 (red) docked with HLA-DR subunits (blue) visualized using ChimeraX. (a) HLA-DRA:ESAT-6. (b) HLA-DRB1:ESAT-6. (c) HLA-DRB3:ESAT-6. (d) HLA-DRB4:ESAT-6. (e) HLA-DRB5:ESAT-6.

Table 3 Binding Free Energy (ΔG) and Dissociation Constant (K_d) Prediction of the Protein-Protein Complexes via PRODIGY

Protein-Protein Complex	ΔG (kcal mol^{-1})	K_d (M) at 37°C	Rank
HLA-DRB3:ESAT-6	-11.4	9.4×10^{-9}	1
HLA-DRB1:ESAT-6	-10.7	2.9×10^{-8}	2
HLA-DRB4:ESAT-6	-10.3	5.4×10^{-8}	3
HLA-DRB5:ESAT-6	-9.7	1.4×10^{-7}	4
HLA-DRA:ESAT-6	-9.2	3.5×10^{-7}	5

Further analysis of the parameters revealed that the observed ΔG values exhibited minimal variation ($\bar{x}$ = -10.26 kcal mol^{-1}; sx = 0.86 kcal mol^{-1}; CV = 8%). However, the dissociation constants showed high dispersion relative to the mean ($\bar{x}$ = 1.1648×10^{-7} M; sx = 1.40×10^{-7} M; CV = 120%) indicating substantial variability in binding affinity values. This indicated that even though ESAT-6 formed a uniformly stable interaction with the HLA-DR subunits, the complexes had varying dissociation constants possibly caused by the different orientations and poses the proteins were positioned at [28].

The β chain of HLA-DR subunit exhibited polymorphism, which affected each bound peptide [43]. This heterodimer was composed of α and β chains with two chains forming an antigenic binding cleft that had eight β-sheets between two antiparallel α-helices. The α-chains, being conserved, were similar among HLA-DR molecules. On the other hand, β-chains gave rise to various HLA-DR subtypes as the binding cleft in this region held different antigenic peptide lengths [44]. The polymorphisms in the HLA-DRB loci were analogous to each other. However, HLA-DRB1 was expressed five times higher with over 500 alleles [45] and was the most polymorphic in the HLA region [46]. It was part of the genetic makeup of every individual as it was always present in the HLA-DR haplotype [43]. The HLA-DRB genes were analogous to

ISSN: 1343-4292
Volume 142, Issue 09, September, 2024

each other and polymorphic, yet they all shared structural similarities in their binding cleft. This then explained the minimal variation observed in the obtained high binding affinities.

In contrast, HLA-DRA:ESAT-6 had the lowest free energy (-9.2) and had the highest dissociation constant (3.5×10^{-7}) among the docked HLA-DR subunits. It had the lowest binding affinity predicted out of all the docked complexes. This complex is influenced in activating the immunological response of a body [46]. HLA-DRA was typically invariant with minimal polymorphism when compared to HLA-DRB subunits, which were polymorphic with different gene and allele variations [47]. Since it had the lowest binding affinity out of the other complexes, it implies that its α chains had less binding affinity towards antigens and had a lesser contribution to antigen binding during antigen presentation yet with a function to provide stability instead [47].

Moreover, HLA-DRB3 had the highest binding affinity, thus indicating a stronger and stable binding compared to the other docked protein-protein complexes. Since unstable complexes cause premature dissociation and insufficient T cell activation, this binding stability is a vital factor for maintaining the integrity of the immune response over time. Furthermore, sustained engagement with T-cell receptors was made possible by the complex's strong binding, which is also vital for efficient signaling and T cell activation [48]. Certain HLA-DRB3 alleles have been linked to a number of diseases [43]. The high binding affinity of HLA-DRB3 impacted the immune system's capacity for recognition of self-versus nonself-antigens, hence influencing susceptibility to certain diseases.

3.3.1.1 Interfacial Contacts

Table 4 Specific ICs between Residues of ESAT-6 with HLA-DR subunits ranked from highest to lowest binding affinity

Protein-Protein Complex	ICs charged-charged	ICs charged-polar	ICs charged-apolar	ICs polar-polar	ICs polar-apolar	ICs apolar-apolar	Total ICs
HLA-DRB3: ESAT-6	1	6	13	5	25	29	79
HLA-DRB1: ESAT-6	1	8	16	4	20	27	76
HLA-DRB4: ESAT-6	0	3	10	3	21	29	66
HLA-DRB5: ESAT-6	0	4	11	5	19	33	72
HLA-DRA: ESAT-6	2	8	16	4	18	26	74

As reported in Table 4, PRODIGY showed the number of ICs made at the protein-protein complex interface within a 5.5 Å distance threshold, which correlated with the binding affinity and largely influenced the interaction. The results showed no significant differences observed when it came to the predicted ICs. The observed values from the binding affinity results were not significantly different to one another but it suggests that the binding properties were influenced by specific ICs present in the protein-protein complex [49].

Additionally, from the previous discussion on the binding affinity, it was shown that the strongest protein-protein complex was HLA-DRB3:ESAT-6. As shown in Table 4, this was consistent with the results in ICs

since HLA-DRB3:ESAT-6 had the most apolar-apolar contacts, one charged-charged interaction, and five polar-polar interactions. A major contributor to the binding affinity were the apolar-apolar ICs as the polar solvent surrounding the complex is in to force the nonpolar residues to aggregate at its center. Hydrophobic interactions were shown to be generally enriched in high-efficiency ligands [50], which implies that the protein-ligand complex had higher stability due to the apolar-apolar interactions between their complexes.

Moreover, the complex's affinity was strengthened by interactions between charged residues and polar groups, especially when hydrogen bonds were formed. Essentially, even at a longer distance, like what was used in PRODIGY, charge-charge interactions were still significantly influential. The formation of hydrogen bonds also made polar-polar contacts ideal for binding, strengthening its influence on the complex's binding affinity [49]. Even though charged and polar group contacts represented only a small portion of the ICs, their presence still influenced the binding capacity of HLA-DRA:ESAT-6 which contributed to its low binding affinity. Although the complex ranked last, the close binding affinity scores between all the protein-protein complexes showed that all HLA-DR subunits had probable effects in the immune response when binded with ESAT-6. All HLA-DR molecules had an invariant α chain in common, and the variations in the highly polymorphic β chain explained the various binding motifs of the DR molecules. This explained why there were small differences in their binding affinities, which altered the way they bind with ESAT-6 [51].

3.3.1.2 Binding Motifs

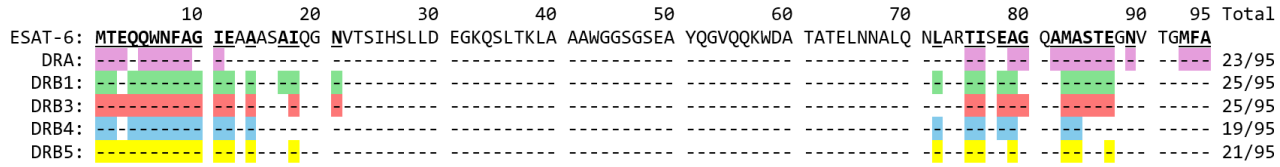

Figure 6 Binding Motif of ESAT-6 with HLA-DRA (purple), HLA-DRB1 (green), HLA-DRB3 (red), HLA-DRB4 (blue) and HLA-DRB5 (yellow), with residues involved in binding (underlined).

Figure 6 showed the highlighted residues of ESAT-6 that were involved in binding with the HLA-DR subunits as provided by PRODIGY. The involved residues were mostly at the terminal ends of the protein starting from Met-1 to Asn-21 at the N-terminal and Leu-72 to Ala-95 at the C-terminal. ESAT-6 uses its N-terminal and C-terminal regions for binding to all of these subunits with more residues involved at the N-terminal end. These regions were disordered but flexible, which was the reason for the strong binding affinity as these arms change their conformation to adapt a more favorable pose when binding. These regions were already theorized to be useful in ESAT-6's primary function as a transmembrane protein and were used to anchor the protein to the cellular membrane's lipid bilayer [37]. Conversely, the rest of the protein did not interact with HLA-DR subunits. This implied that it was more thermodynamically favorable for ESAT-6 to bind to HLA-DR subunits via conformational flexibility than to rely on hydrophobic interactions.

ISSN: 1343-4292
Volume 142, Issue 09, September, 2024

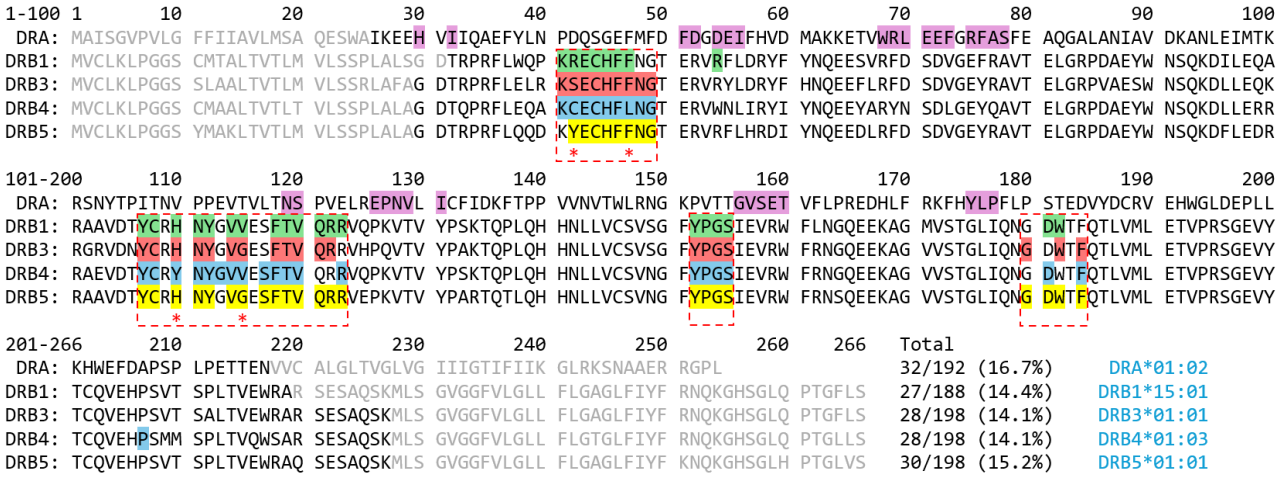

Figure 7 Multiple Sequence Alignment of HLA-DR subunits with highlighted residues involved in binding with ESAT-6. Conserved functional regions are boxed with notable polymorphic residues (*), and non-modeled regions are shown as gray text.

Figure 7 emphasized the residues of each HLA-DR subunit that binds to ESAT-6, which showed distinct locations as to where ESAT-6 bound to. The most notable were the four distinct regions (red boxes) that were conserved across HLA-DRB subunits. Residues 41-49 and 106-123 were mostly conserved with each region only having two polymorphic residues, but with a less consistent binding motif. Residues 152-155 were completely conserved and exhibited the most consistent binding motif. Also, residues 180-184 were completely conserved yet with the least consistent binding motif. There were also two outliers: Arg-54 (HLA-DRB1) and Pro-107 (HLA-DRB4). Since these subunits were homologous, their functional regions were mostly retained with minimal differences and outliers. The similarity of these binding sites reflected on each of the complex's binding affinity having low variability. Conversely, HLA-DRA had the most residues involved (16.7%) but had the weakest binding affinity out of all five complexes. This further implied that the binding affinity of these proteins was more likely linked to what residue interaction was present rather than the number of residues involved.

HLA-DR were essential for antigen presentation to T-cell receptors. The invariant chain regulated this process by preventing premature peptide binding [52]. The findings of this study indicated that ESAT-6 bound strongly to HLA-DR subunits, potentially targeting key regions involved in protein-protein interactions which gave it the ability to disrupt the structural integrity of HLA-DR, impair antigen presentation, and ultimately weaken the immune response against *M. tb* [53].

4. Conclusion

Various properties and characteristics of ESAT-6 in *M. tb* have been investigated along with its binding capacity to MHC class II HLA-DR subunits. Nine residues were buried falling below the 25% threshold. The N- and C-terminal ends were the most exposed regions. Exposed residues are crucial in molecular recognition, binding, and protein complex formation influencing its function. Its estimated half-life was approximately 30 hours in mammalian reticulocytes, which allows it to persist within the host and interfere in immunologic responses.

For model validation of the ESAT-6, SWISS-MODEL's quality metrics were utilized, namely, the Ramachandran Plot Analysis, MolProbity, QMEAN and QMEANDisCo and NetSurfP 3.0. The model rendered was shown to mostly be within the parameters, thus making the model reliable though with minor

discrepancies.

Furthermore, sequence-based and structural analysis of ESAT-6 provided a crucial perspective into its functional properties, adaptability, and potential role in pathogenicity. Through this analysis, several key findings were identified including its conformational flexibility and hydrophobicity. ESAT-6's amino acid composition was predominated by alanine and glycine, which contributed to the protein's flexibility allowing conformational changes. Moreover, the disordered but flexible terminal regions served an important role in binding and interacting with other molecules. Additionally, the hydrophobicity of these regions showed properties akin to transmembrane peptides. It revealed that ESAT-6 exhibited a distinct hydrophobic and hydrophilic side that facilitated its interactions with other proteins. Also, the major presence of alanine and glutamine contributed to the protein's hydrophobicity and hydrophilicity, respectively. Aliphatic molecules comprised the stable hydrophobic core of the protein. These residues have a tendency to form transmembrane helices, which then establish pores essential for the potency of ESAT-6. Alternately, hydrophilic regions were a factor for its aqueous solubility.

Furthermore, the binding capacity of ESAT-6 to MHC class II HLA-DR subunits showed implications of the development and virulence of *M. tb*. The results showed that HLA-DRB3:ESAT-6 had the highest binding affinity with a free energy of -11.4 kcal mol^{-1}, indicating a stronger and stable binding affinity compared to the other docked proteins. This proved an interaction with the host's immune response. In the case of the HLA-DRB subunit, the results obtained have minimal variations on account of them being polymorphisms. Moreover, the strong interactions of HLA-DR subunits and the ESAT-6 suggested that the protein potentially targets these subunits to disrupt its antigen presentation, and by extension, the host immune response. A major contribution to this binding affinity was the predominant apolar-apolar ICs that stabilized the complex. The locations of these ICs showed a consistent motif as ESAT-6 contort its terminal ends which tend to bind on the same residues on HLA-DRB subunits.

5. References

[1] Churchyard, G., Kim, P., Shah, N. S., Rustomjee, R., Gandhi, N., Mathema, B., Dowdy, D., Kasmar, A., & Cardenas, V. (2017). What we Know about tuberculosis Transmission: An overview. The Journal of Infectious Diseases, 216. https://doi.org/10.1093/infdis/jix362

[2] World Health Organization. (2024). Tuberculosis. https://www.who.int/news-room/fact-sheets/detail/tuberculosis

[3] Jha, V., Pal, R., Kumar, D., & Mukhopadhyay, S. (2020). ESAT-6 Protein of Mycobacterium tuberculosis Increases Holotransferrin-Mediated Iron Uptake in Macrophages by Downregulating Surface Hemochromatosis Protein HFE. The Journal of Immunology, 205(11), pp. 3095–3106. https://doi.org/10.4049/jimmunol.1801357

[4] Anes, E., Pires, D., Mandal, M., & Azevedo-Pereira, J. M. (2023). ESAT-6 a Major Virulence Factor of Mycobacterium tuberculosis. Biomolecules, 13(6), 968. https://doi.org/10.3390/biom13060968

[5] Stevens, C. D., & Miller, L. E. (2017). Clinical Immunology and Serology: A Laboratory Perspective (4th ed.) [Book]. F. A. Davis.

[6] Lee, Y., Hyun, Y., Jo, H., Baek, I., Kim, S., Sohn, H., & Kim, T. (2022). Comprehensive analysis of mycobacterium tuberculosis antigen-specific CD4+ T cell responses restricted by single HLA class II

allotype in an individual. Frontiers in Immunology, 13. https://doi.org/10.3389/fimmu.2022.897781

[7] The UniProt Consortium. (2025). UniProt: the Universal Protein Knowledgebase in 2025, Nucleic Acids Research, 53(1), pp. 609–617, https://doi.org/10.1093/nar/gkae1010

[8] Studer, G., Rempfer, C., Waterhouse, A. M., Gumienny, R., Haas, J., & Schwede,T. (2019). QMEANDisCo—distance constraints applied on model quality estimation. Bioinformatics, 36(6), pp. 1765–1771. https://doi.org/10.1093/bioinformatics/btz828

[9] Waterhouse, A., Bertoni, M., Bienert, S., Studer, G., Tauriello, G., Gumienny, R., Heer, F. T., De Beer, T. a. P., Rempfer, C., Bordoli, L., Lepore, R., & Schwede, T. (2018). SWISS-MODEL: homology modelling of protein structures and complexes. Nucleic Acids Research, 46(W1), pp. W296–W303. https://doi.org/10.1093/nar/gky427

[10] Rao, S., Sayeeda, M., Prakash, T., & Ap, P. (2020). Construction of Computational 3D Structures of Protein Drug Targets of Mycobacterium Tuberculosis. Asian Journal of Pharmaceutical and Clinical Research. http://dx.doi.org/10.22159/ajpcr.2020.v13i11.39242

[11] Shahjahan, M., & Rahman, S. (2018). Insilico Analysis of γ- Aminobutaric Acid Transaminase (GABA-T) of Brassica napus (Rape). Journal of Advanced Biotechnology and Experimental Therapeutics, 2(1). http://dx.doi.org/10.5455/jabet.2018.d18

[12] Høie, M. H., Kiehl, E. N., Petersen, B., Nielsen, M., Winther, O., Nielsen, H., Hallgren, J., & Marcatili, P. (2022). NetSurfP-3.0: accurate and fast prediction of protein structural features by protein language models and deep learning. Nucleic Acids Research, 50(W1), pp. W510–W515. https://doi.org/10.1093/nar/gkac439

[13] Gasteiger, E., Hoogland, C., Gattiker, A., Duvaud, S., Wilkins, M. R., Appel, R. D., & Bairoch, A. (2005). Protein Identification and Analysis Tools on the Expasy Server. John M. Walker (ed): The Proteomics Protocols Handbook, Humana Press, pp. 571-607. https://link.springer.com/book/10.1385/1592598900

[14] Hallgren, J., Tsirigos, K. D., Pedersen, M. D., Armenteros, J. J. A., Marcatili, P., Nielsen, H., Krogh, A., & Winther, O. (2022). DeepTMHMM predicts alpha and beta transmembrane proteins using deep neural networks. https://doi.org/10.1101/2022.04.08.487609

[15] Jones, G., Jindal, A., Ghani, U., Kotelnikov, S., Egbert, M., Hashemi, N., Vajda, S., Padhorny, D., & Kozakov, D. (2022). Elucidation of protein function using computational docking and hotspot analysis by ClusPro and FTMap. Acta Crystallographica Section D Structural Biology, 78(6), pp. 690–697. https://doi.org/10.1107/s2059798322002741

[16] Desta, I. T., Porter, K. A., Xia, B., Kozakov, D., & Vajda, S. (2020). Performance and its limits in rigid body Protein-Protein docking. Structure, 28(9), pp. 1071-1081.e3. https://doi.org/10.1016/j.str.2020.06.006

[17] Vajda, S., Yueh, C., Beglov, D., Bohnuud, T., Mottarella, S. E., Xia, B., Hall, D. R., & Kozakov, D. (2016). New additions to the ClusPro server motivated by CAPRI. Proteins Structure Function and Bioinformatics, 85(3), pp. 435–444. https://doi.org/10.1002/prot.25219

[18] Kozakov, D., Hall, D. R., Xia, B., Porter, K. A., Padhorny, D., Yueh, C., Beglov, D., & Vajda, S. (2017). The ClusPro web server for protein–protein docking. Nature Protocols, 12(2), pp. 255–278. https://doi.org/10.1038/nprot.2016.169

[19] Kozakov, D., Beglov, D., Bohnuud, T., Mottarella, S. E., Xia, B., Hall, D. R., & Vajda, S. (2013). How good is automated protein docking? Proteins Structure Function and Bioinformatics, 81(12), pp. 2159–2166. https://doi.org/10.1002/prot.24403

[20] Honorato, R. V., Koukos, P. I., Jiménez-García, B., Tsaregorodtsev, A., Verlato, M., Giachetti, A., Rosato, A., & Bonvin, A. M. J. J. (2021). Structural biology in the clouds: the WENMR-EOSC ecosystem. Frontiers in Molecular Biosciences, 8. https://doi.org/10.3389/fmolb.2021.729513

[21] Vangone, A., & Bonvin, A. M. (2015). Contacts-based prediction of binding affinity in protein–protein complexes. eLife, 4. https://doi.org/10.7554/elife.07454

[22] Xue, L. C., Rodrigues, J. P., Kastritis, P. L., Bonvin, A. M., & Vangone, A. (2016). PRODIGY: a web server for predicting the binding affinity of protein–protein complexes. Bioinformatics, 32(23), pp. 3676–3678. https://doi.org/10.1093/bioinformatics/btw514

[23] Osilla, E. V., Marsidi, J. L., Shumway, K. R., & Sharma, S. (2023). Physiology, temperature regulation. StatPearls - NCBI Bookshelf. https://www.ncbi.nlm.nih.gov/books/NBK507838/

[24] Meng, E. C., Goddard, T. D., Pettersen, E. F., Couch, G. S., Pearson, Z. J., Morris, J. H., & Ferrin, T. E. (2023). UCSF ChimeraX: Tools for structure building and analysis. Protein Science, 32(11). https://doi.org/10.1002/pro.4792

[25] Pettersen, E. F., Goddard, T. D., Huang, C. C., Meng, E. C., Couch, G. S., Croll, T. I., Morris, J. H., & Ferrin, T. E. (2020). UCSF ChimeraX: Structure visualization for researchers, educators, and developers. Protein Science, 30(1), pp. 70–82. https://doi.org/10.1002/pro.3943

[26] Goddard, T. D., Huang, C. C., Meng, E. C., Pettersen, E. F., Couch, G. S., Morris, J. H., & Ferrin, T. E. (2017). UCSF ChimeraX: Meeting modern challenges in visualization and analysis. Protein Science, 27(1), pp. 14–25. https://doi.org/10.1002/pro.3235

[27] Mier, P., Elena-Real, C. A., Cortés, J., Bernadó, P., & Andrade-Navarro, M. A. (2022). The sequence context in poly-alanine regions: Structure, function and conservation. Bioinformatics, 38(21), pp. 4851–4858. https://doi.org/10.1093/bioinformatics/btac610

[28] Bates, T. A., Trank-Greene, M., Nguyenla, X., Anastas, A., Gurmessa, S. K., Merutka, I. R., Dixon, S. D., Shumate, A., Groncki, A. R., Parson, M. A., Ingram, J. R., Barklis, E., Burke, J. E., Shinde, U., Ploegh, H. L., & Tafesse, F. G. (2024). ESAT-6 undergoes self-association at phagosomal pH and an ESAT-6-specific nanobody restricts M. tuberculosis growth in macrophages. eLife, 12. https://doi.org/10.7554/elife.91930.3

[29] Jha, V., Rameshwaram, N. R., Janardhan, S., Raman, R., Sastry, G. N., Sharma, V., Subba Rao, J., Kumar, D., & Mukhopadhyay, S. (2019). Uncovering structural and molecular dynamics of Esat-6:β2M interaction: Asp53 of human β2-microglobulin is critical for the Esat-6:β2M complexation. The Journal of

Immunology, 203(7), pp. 1918–1929. https://doi.org/10.4049/jimmunol.1700525

[30] Passos, B. B. S., Araújo-Pereira, M., Vinhaes, C. L., Amaral, E. P., & Andrade, B. B. (2024). The role of ESAT-6 in tuberculosis immunopathology. Frontiers in Immunology, 15. https://doi.org/10.3389/fimmu.2024.1383098

[31] Senthil, R., Usha, S., & Saravanan, K. M. (2019). Importance of fluctuating amino acid residues in folding and binding of proteins. Avicenna journal of medical biotechnology. https://pmc.ncbi.nlm.nih.gov/articles/PMC6925403/

[32] Almeida, F. C., Sanches, K., Pinheiro-Aguiar, R., Almeida, V. S., & Caruso, I. P. (2021). Protein surface interactions—theoretical and experimental studies. Frontiers in Molecular Biosciences, 8. https://doi.org/10.3389/fmolb.2021.706002

[33] Peng, X., & Sun, J. (2016). Mechanism of ESAT-6 membrane interaction and its roles in pathogenesis of Mycobacterium tuberculosis. Toxicon, 116, pp. 29-34. https://doi.org/10.1016/j.toxicon.2015.10.003

[34] Durell, S. R., & Ben-Naim, A. (2017). Hydrophobic-hydrophilic forces in protein folding. Biopolymers, 107(8). https://doi.org/10.1002/bip.23020

[35] Sanvictores, T., & Farci, F. (2023). Biochemistry, Primary Protein Structure. In StatPearls. StatPearls Publishing LLC. https://europepmc.org/article/NBK/nbk564343#article-126713.r12

[36] Marsh, J. A., & Teichmann, S. A. (2011). Relative Solvent Accessible Surface Area Predicts Protein Conformational Changes upon Binding. Structure, 19(6), 859–867. https://doi.org/10.1016/j.str.2011.03.010

[37] Ma, Y., Keil, V., & Sun, J. (2015). Characterization of Mycobacterium tuberculosis EsxA Membrane Insertion. Journal of Biological Chemistry, 290(11), pp. 7314–7322. https://doi.org/10.1074/jbc.m114.622076

[38] Refai, A., Haoues, M., Othman, H., Barbouche, M. R., Moua, P., Bondon, A., Mouret, L., Srairi-Abid, N., & Essafi, M. (2015). Two distinct conformational states of Mycobacterium tuberculosis virulent factor early secreted antigenic target 6 kDa are behind the discrepancy around its biological functions. FEBS Journal, 282(21), pp. 4114–4129. https://doi.org/10.1111/febs.13408

[39] Kordi, B., Basmenj, E. R., Majidiani, H., Basati, G., Sargazi, D., Nazari, N., & Shams, M. (2023). In Silico Characterization of an Important Metacyclogenesis Marker in Leishmania donovani, HASPB1, as a Potential Vaccine Candidate. BioMed Research International, 2023, pp. 1–13. https://doi.org/10.1155/2023/3763634

[40] Williams, C. J., Headd, J. J., Moriarty, N. W., Prisant, M. G., Videau, L. L., Deis, L. N., Verma, V., Keedy, D. A., Hintze, B. J., Chen, V. B., Jain, S., Lewis, S. M., Arendall, W. B., Snoeyink, J., Adams, P. D., Lovell, S. C., Richardson, J. S., & Richardson, D. C. (2017). Molprobity: More and better reference data for improved all-atom structure validation. Protein Science, 27(1), pp. 293–315. https://doi.org/10.1002/pro.3330

[41] Cruz-Tapias, P., Castiblanco, J., & Anaya, J. (2013). Autoimmunity: From Bench to Bedside. El

Rosario University Press. https://www.ncbi.nlm.nih.gov/books/NBK459467/

[42] Mohanapriya, A., Nandagond, S., Shapshak, P., Kangueane, U., & Kangueane, P. (2010). A HLA-DRB supertype chart with potential overlapping peptide binding function. Bioinformation, 4(7). https://doi.org/10.6026/97320630004300

[43] Faner, R., James, E., Huston, L., Pujol-Borrel, R., Kwok, W. W., & Juan, M. (2010). Reassessing the role of HLA-DRB3 T cell responses: Evidence for significant expression and complementary antigen presentation. European Journal of Immunology, 40(1). https://doi.org/10.1002/eji.200939225

[44] Kongkaew, S., Rungrotmongkol, T., Punwong, C., Noguchi, H., Takeuchi, F., Kungwan, N., Wolschann, P., & Hannongbua, S. (2019). Interactions of HLA-DR and topoisomerase I epitope modulated genetic risk for systemic sclerosis. Scientific Reports, 9(1). https://doi.org/10.1038/s41598-018- 37038-z

[45] Gouw, J. W., Jo, J., Meulenbroek, L. a. P. M., Heijjer, T. S., Kremer, E., Sandalova, E., Knulst, A. C., Jeurink, P. V., Garssen, J., Rijnierse, A., & Knippels, L. M. J. (2018). Identification of peptides with tolerogenic potential in a hydrolysed whey-based infant formula. Clinical & Experimental Allergy, 48(10), pp. 1345–1353. https://doi.org/10.1111/cea.13223

[46] Hassan, M. M., Hussain, M. A., Ali, S. S., & Mahdi, M. A. (2023). In Silico Analysis: HLA-DRB1 gene's variants and their clinical impact. Cell Transplantation, 32. https://doi.org/10.1177/09636897231184473

[47] Abualrous, E. T., Stolzenberg, S., Sticht, J., Wieczorek, M., Roske, Y., Günther, M., Dähn, S., Boesen, B. B., Calvo, M. M., Biese, C., Kuppler, F., MedinaGarcía, Á., Álvaro-Benito, M., Höfer, T., Noé, F., & Freund, C. (2023). MHC-II dynamics are maintained in HLA-DR allotypes to ensure catalyzed peptide exchange. Nature Chemical Biology, 19(10), pp. 1196–1204. https://doi.org/10.1038/s41589-023-01316-3

[48] Szeto, C., Bloom, J. I., Sloane, H., Lobos, C. A., Fodor, J., Jayasinghe, D., Chatzileontiadou, D. S. M., Grant, E. J., Buckle, A. M., & Gras, S. (2020). Impact of HLA-DR antigen binding cleft rigidity on T cell recognition. International Journal of Molecular Sciences, 21(19), 7081. https://doi.org/10.3390/ijms21197081

[49] Zhou, H., & Pang, X. (2018). Electrostatic interactions in protein structure, folding, binding, and condensation. Chemical Reviews, 118(4), pp. 1691–1741. https://doi.org/10.1021/acs.chemrev.7b00305

[50] De Freitas, R. F., & Schapira, M. (2017). A systematic analysis of atomic protein– ligand interactions in the PDB. MedChemComm, 8(10), pp. 1970–1981. https://doi.org/10.1039/c7md00381a

[51] Kaabinejadian, S., Barra, C., Alvarez, B., Yari, H., Hildebrand, W. H., & Nielsen, M. (2022). Accurate MHC motif deconvolution of immunopeptidomics data reveals a significant contribution of DRB3, 4 and 5 to the total DR immunopeptidome. Frontiers in Immunology, 13. https://doi.org/10.3389/fimmu.2022.835454

[52] Wang, N., Waghray, D., Caveney, N. A., Jude, K. M., & Garcia, K. C. (2024). Structural insights into human MHC-II association with invariant chain. Proceedings of the National Academy of Sciences, 121(19). https://doi.org/10.1073/pnas.2403031121

ISSN: 1343-4292
Volume 142, Issue 09, September, 2024

[53] Sreejit, G., Ahmed, A., Parveen, N., Jha, V., Valluri, V. L., Ghosh, S., & Mukhopadhyay, S. (2014). The ESAT-6 Protein of Mycobacterium tuberculosis Interacts with Beta-2-Microglobulin (β2M) Affecting Antigen Presentation Function of Macrophage. PLoS Pathogens, 10(10). https://doi.org/10.1371/journal.ppat.1004446